Available online at www.sciencedirect.com

SciVerse ScienceDirect

Ceramics International 39 (2013) 2215–2222

CERAMICS INTERNATIONAL

www.elsevier.com/locate/ceramint

Preparation, microstructure, and mechanical properties of ZrB_2-based ceramics with layered $Zr_2Al_4C_5$ inclusions

Qilong Guo, Junguo Li*, Qiang Shen, Lianmeng Zhang

State Key Laboratory of Advanced Technology for Materials Synthesis and Processing, Wuhan University of Technology, Wuhan 430070, PR China

Received 6 July 2012; received in revised form 13 August 2012; accepted 13 August 2012
Available online 18 August 2012

Abstract

$ZrB_2/Zr_2Al_4C_5$ composite ceramics with different volume contents of $Zr_2Al_4C_5$ formed in situ were fabricated by the spark plasma sintering technique at 1800 °C. The content of $Zr_2Al_4C_5$ was found to have an evident effect on the preparation, phase constitution, microstructure as well as the mechanical properties of $ZrB_2/Zr_2Al_4C_5$ ceramics. The results indicated that sinterability of the composites was remarkably improved by the addition of $Zr_2Al_4C_5$ compared to the single-phase ZrB_2 ceramic. The microstructure of the resulting composites was fine and homogeneous, the average grain size of the ZrB_2 decreased, and the average aspect ratio of the $Zr_2Al_4C_5$ increased with the increase in the amount of $Zr_2Al_4C_5$. As the content of $Zr_2Al_4C_5$ increased, both the Vickers hardness and Young's modulus of the composites first increased and then decreased. The fracture toughness of the ZrB_2–40 vol% $Zr_2Al_4C_5$ composite was 4.25 MPa $m^{1/2}$, which increased by approximately 70% compared to the monolithic ZrB_2 ceramic. The improvement was mainly attributed to the toughening mechanisms such as the layered structure toughening, crack deflection and crack bridging, caused by the in situ formed layered $Zr_2Al_4C_5$ inclusions.

Keywords: A. Sintering; B. X-ray methods; C. Mechanical properties; C. Toughness and toughening

1. Introduction

Zirconium diboride (ZrB_2), belonging to ultra-high-temperature ceramics (UHTCs), is currently expected to be a potential candidate material for aerospace applications, such as rocket engines and thermal protection structures for leading-edge parts on hypersonic re-entry space vehicles, attributing to their high melting point, high thermal and electrical conductivities, good chemical stability, low theoretical density, and good chemical inertness [1–6].

However, there are two main bottleneck problems that limit the development of ZrB_2 ceramics. On one hand, the densification of ZrB_2, with additives, typically requires hot pressing at 2100–2300 °C due to its strong covalent bonding and the presence of surface oxide impurities [7]. On the other hand, ZrB_2 is very brittle and does not have sufficient toughness, strength, and thermal shock resistance to be used successfully for aerospace applications [8]. Considerable efforts have been made to improve the sinterability and the mechanical properties of ZrB_2-based composite ceramics. These efforts include the addition of second phases, various nitrides, silicides, such as $MoSi_2$, $ZrSi_2$, HfN, BN, AlN, ZrC, ZrO_2 [1,9–13], or combinations of various second phases. Among these second phases, SiC is a typical second phase particle for ZrB_2, which can not only enhance the oxidation resistance of ZrB_2 ceramics, but also improve the sinterability and fracture toughness of the ZrB_2-based composites [4]. Unfortunately, the ZrB_2–SiC composites have appreciable shortcomings, for instance, the low fracture toughness and the poor thermal shock resistance limit its wider application.

Recent studies showed that the incorporation of ceramic inclusions with different shapes and sizes, including SiC whisker [14], SiC chopped fiber [15], ZrO_2 fiber [16], nanosized SiC [17], short carbon fiber [18], carbon nanotube [19], was attributed to the combination of debonding, pull-out, and bridging of these reinforcements as well as enhanced crack deflection and crack pinning. Meanwhile,

*Corresponding author. Tel./fax: +86 27 87217002.
E-mail address: guoqilongfgm@whut.edu.cn (Q. Guo).

0272-8842/$ - see front matter
http://dx.doi.org/10.1016/j.ceramint.2012.08.036

some researches had been done through the fabrication of laminated-type architectures with compressive stresses [20,21] or of complex cell-type architectures [22] which were the feasible strategies to reach the higher fracture toughness. It has been widely used that the second phase additions with a higher aspect ratio (e.g., flakes or rods/whiskers) are used as toughening materials incorporated with the ZrB_2-based composites.

Recently, Zheng et al. [23] investigated that the densification and mechanical properties of TiB_2 using Ti_3AlC_2 as a sintering aid. The improvement was mainly attributed to the elimination of the oxides layer on the surface of the initial TiB_2 powders by active Al, which came from the decomposition of Ti_3AlC_2. In another study, Chin et al. [24] reported that the addition of a ductile Ti_3SiC_2 phase can enhance the toughness of Al_2O_3 ceramic. Therefore, due to its characters of superior strength, specific stiffness, high fracture toughness, excellent oxidation resistance and anisotropic microstructure consisting of elongated and rod-like and/or plate-like grains [25,26], the layered structure $Zr_2Al_4C_5$ was a very promising alternative for improving the sinterability and enhancing the toughness of ZrB_2 ceramics [27].

In this study, the structure of ZrB_2 particles coated by Zr, Al metal was first prepared using high-energy ball milling. Therefore, the aims of this work are as follows: (1) to explore the possibility of sintering ZrB_2 using $Zr_2Al_4C_5$ as a new sintering aid, (2) to describe the influence of the $Zr_2Al_4C_5$ content on the densification, microstructures and mechanical properties of the prepared composites, and (3) to investigate systematically the effect of the average aspect ratio of $Zr_2Al_4C_5$ grains on the mechanical properties of the composites and discuss the toughening mechanism.

2. Experimental procedure

The raw materials used in the present study were as follows: commercially available ZrB_2 powder (10 μm, > 99.5%, Alfa Aesar Co. Ltd., Beijing), Zr powders (purity > 99.9%, 10 μm, Beijing mountain technical development center for non-ferrous metals, China), Al powders (purity > 99.99%, 8 μm, Shanghai chemical reagents of Chinese medicine group, China), graphite powders (purity > 99.9%, 1 μm, Shanghai capable graphite Co. Ltd., China).

The designed compositions of $ZrB_2/Zr_2Al_4C_5$ ceramics in the present work were shown in Table 1. The powder mixtures of ZrB_2 plus Zr plus Al were high-energy ball mixed for 4 h in a steel bottle using WC balls. The ZrB_2 particles were subsequently coated with Zr, Al metal and/or Zr–Al alloys, due to the fact that Zr and Al are ductile metals and ZrB_2 is brittle powder. The oxygen contents were measured using oxygen analyzer instrument (Model TC600, Leco, America). Powder samples were dispersed in ethanol to minimize agglomeration during analysis and the particle size of the milled powder was measured using a laser diffraction particle size analyzer (Mastersizer 2000).

After ball mixing, the mixture plus graphite were mixed in an agate mortar. The content of $Zr_2Al_4C_5$ in $ZrB_2/Zr_2Al_4C_5$ composites was adjusted by controlling the amounts of Zr, Al and C. The mixture of initial powders was poured into a graphite die with graphite foil and sintered using a SPS system (model-1050, Sumitomo Coal Mining Co. Ltd., Tokyo).

The temperature was measured by an optical pyrometer focused on the surface of the graphite die. The samples were heated to 600 °C at a rate of 300 °C/min, then with an average heating rate of 100 °C/min maintained up to 1800 °C. And then the temperature holds constant for 3 min. The sample was cooled naturally after the sintering period finished. A uniaxial pressure of 20 MPa and a vacuum atmosphere were applied from the start to the end of the sintering cycle.

The bulk density and open porosity of the sintered products were determined by Archimedes' immersion method with water as the immersing medium. The phase composition was analyzed by the X-ray diffraction (XRD) using a Rigaku Ultima III diffractometer. Cu radiation is used and operated at 40 KV and 40 mA. The microstructure of the polished and fractured surfaces was analyzed by the scanning electron microscopy (SEM, Model S-3400, Hitachi, Japan) equipped with energy-dispersive X-ray spectroscopy (EDS). The grain size of samples was determined through image analysis on SEM micrographs of polished surfaces using a commercial software program (Image-Pro Plus 6.0, Media Cybernetics, Silver Springs, MD, USA). The average grain size was estimated by measuring at least 100 ZrB_2 or $Zr_2Al_4C_5$ grains.

Young's modulus (E) of the composites was determined using an ultrasonic equipment (Panametrics 5072PR) with a fundamental frequency of 20 MHz. The Vickers hardness (H_V) and fracture toughness (K_{IC}) were measured using a Vickers indenter (Wolpert 430SVD, USA). Each polished sample was indented at five locations with a 98N load for 15 s. The fracture toughness was calculated using the following equation [28]:

$$K_{IC} = 0.0264a\left(\frac{EP}{c^3}\right)^{1/2} \quad (1)$$

where E is the Young's modulus, P the load, $2a$ the indentation diagonal length, and $2c$ the crack length. If the ratio of the crack length to indentation length (c/a) is smaller than 2.3, or if there is crack branching, the data are rejected.

3. Results and discussion

Fig. 1 shows the XRD patterns of $ZrB_2/Zr_2Al_4C_5$ composites with different volume contents of $Zr_2Al_4C_5$. It was clear that all the composites with different contents of $Zr_2Al_4C_5$ were mainly composed of ZrB_2 and $Zr_2Al_4C_5$, except for ZA0 sample, which indicated that the $Zr_2Al_4C_5$ phase was fabricated successfully by the in situ reactive

Table 1
Composition, characteristics of the starting powders and measured grain sizes of $ZrB_2/Zr_2Al_4C_5$ ceramics.

Samples	Composition (vol%)		Oxygen content of milled powders (wt%)	Average ZrB_2 size (μm)	Average $Zr_2Al_4C_5$ size (μm)	
	ZrB_2	$Zr_2Al_4C_5$			*d* (μm)	Aspect ratio
Z	100	0	2.6	–	–	–
ZA0	100	0	3.8	6.9 ± 0.7	–	–
ZA1	90	10	3.1	4.9 ± 0.5	1.7 ± 0.1	4
ZA2	80	20	3.2	4.1 ± 0.8	3.3 ± 0.2	4.5
ZA3	70	30	3.8	3.9 ± 0.7	2.7 ± 0.2	8
ZA4	60	40	4.3	3.7 ± 0.6	1.9 ± 0.1	8.5

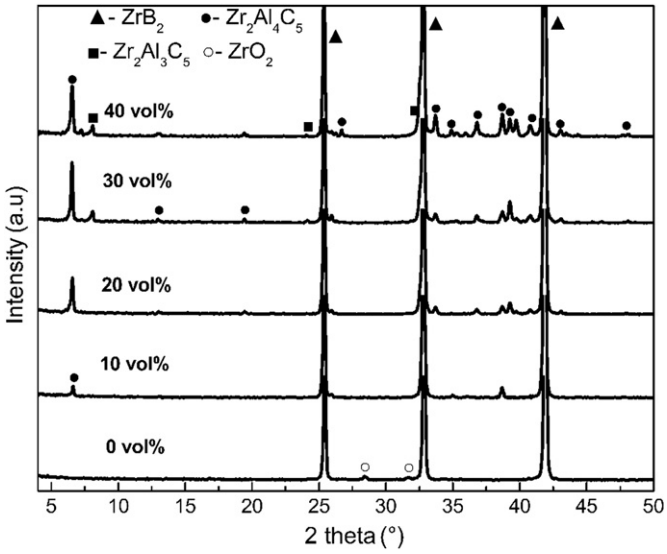

Fig. 1. X-ray diffraction patterns of the $ZrB_2/Zr_2Al_4C_5$ composites.

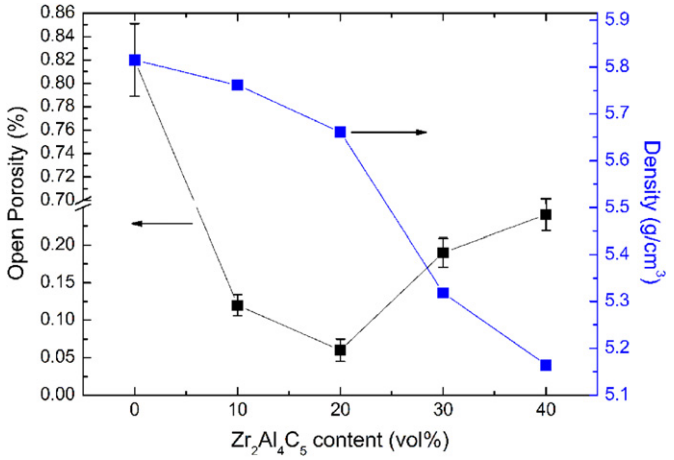

Fig. 2. The curve of the open porosity and density versus $Zr_2Al_4C_5$ content in $ZrB_2/Zr_2Al_4C_5$ composites.

spark plasma sintering using Zr, Al and graphite powders at 1800 °C. The peak intensity of $Zr_2Al_4C_5$ in all samples increased with the increase in theoretical content of $Zr_2Al_4C_5$. Other impurity phases such as $Zr_2Al_3C_5$ were also observed in the ZA3 and ZA4 samples due to the volatilization of Al during the sintering process and $Zr_2Al_4C_5$ had decomposed into $Zr_2Al_3C_5$ and Al because of the fast diffusion of Al at high temperatures [29].

The diffraction peak of ZrO_2 phase was detected in monolithic ZrB_2, as oxygen impurities most likely take the form of ZrO_2 and B_2O_3 on the surface of the ZrB_2 powders during attrition milling [30]. However, the diffraction peak of ZrO_2 disappeared when the $Zr_2Al_4C_5$ phase was produced in the samples. This was because the addition of carbon from the starting powders removed the oxygen impurities based on the following reaction [30]:

$$ZrO_2 + B_2O_3 + 5C \rightarrow ZrB_2 + 5CO \quad (2)$$

The oxygen contents increased from 3.8 wt% in the ZA0 powder to 4.3 wt% in the ZA4 powder, as shown in Table 1. The increased O was thought to be from the formation the ZrO_2, B_2O_3 and Al_2O_3 on the exposed surface of the ZrB_2, Zr and Al powders during milling process in air [31]. Previous studies have shown that oxygen impurities enhanced particle coarsening during heating, which impeded the densification, and impacted the microstructure and mechanical properties of the ceramics. Therefore, some authors have asserted the cleaning of the ZrB_2 surface powder particles from oxygen as the primary step for obtaining a highly dense body [32].

Fig. 2 shows the curve of the open porosity and density versus $Zr_2Al_4C_5$ content in $ZrB_2/Zr_2Al_4C_5$ composites. It can be seen that only 0.82% of the open porosity can be obtained for the monolithic ZrB_2. The high open porosity was mainly attributed to low sinterability at such a low temperature. Compared to the open porosity (10.8%) of as-received powder compacts, the open porosity for attrition-milled was lower, since particle size reduction was necessary to promote densification. When the starting powders were attrition milled for 4 h, its surface area increased and the calculated equivalent particle size decreased from 10 μm for the as-received ZrB_2 powder to 2.5 μm for the milled powder. It was thought that the reduction of the particle size would increase the surface area, thus increasing the driving force for sintering.

Based on the open porosity and XRD results, it can be demonstrated that oxygen contents had a significant impact on the densification of ZrB_2. However, compared to ZA0 sample, the open porosity of the samples remarkably decreased when $Zr_2Al_4C_5$ was added. When 20 vol%

$Zr_2Al_4C_5$ was added, the open porosity can reach 0.06%. These results indicated that $Zr_2Al_4C_5$ can effectively improve the densification behavior of ZrB_2. This can be attributed to the reaction of carbon with these oxide impurities that promoted the densification of ZrB_2 particles and provided a higher driving force for sintering. On the other hand, with the increasing sintering temperature, activation of Al during the sintering process occurs, which came from the presence of liquid Al at 1100 °C [25] and the Al_2O_3 layer that existed on the surface of the metal Al powders which can react with oxides (ZrO_2 and B_2O_3) on the surface of ZrB_2 particles to form a Zr–Al–O–B glassy phase. The presence of an intergranular liquid phase favored the process of grain rearrangement and improved the packing density of particles, thereby improving densification [33]. Thus, the in situ formation of $Zr_2Al_4C_5$ during sintering process could make ZrB_2 composites fully sintered by SPS at 1800 °C. The density decreased gradually with the increase of $Zr_2Al_4C_5$ volume content which is shown in Table 1, because the density of $Zr_2Al_4C_5$ (4.5 g/cm^3) is lower than that of ZrB_2 (6.09 g/cm^3).

SEM images of the polished surfaces of the composites with different $Zr_2Al_4C_5$ contents are shown in Fig. 3. The backscattered electron contrast between the ZrB_2 grains and the $Zr_2Al_4C_5$ phase was small due to the small difference in the mean atomic number of ZrB_2 and $Zr_2Al_4C_5$, as shown in Fig. 3(f). It was confirmed by EDS analyses that the large columnar or plate-like gray grains were identified as $Zr_2Al_4C_5$ and the fine bright particles were ZrB_2. As shown in Fig. 3, the large columnar or plate-like gray $Zr_2Al_4C_5$ grains dispersed homogenously in all these composites, which are not only located at the grain boundaries but also contained within them, since no agglomeration was observed. The black phases in the microstructure were the residual porosity or the unreacted materials, such as graphite, Al_4O_4C, Al_4C_3 etc.

According to Fig. 3, the monolithic ZrB_2 ceramic with some small pores was less dense, while the $ZrB_2/Zr_2Al_4C_5$ composites became denser with an increase in the content of $Zr_2Al_4C_5$. The ZrB_2 grain sizes were determined from the SEM images of the polished surface of the $ZrB_2/Zr_2Al_4C_5$ ceramic using an image analysis software. It was found that the grain size of the ZrB_2 grains decreased along with the increasing amount of $Zr_2Al_4C_5$ grains from 0 to 40 vol%. In the case of the monolithic ZrB_2 ceramic, the average grain size of ZrB_2 was 6.9 μm, which was

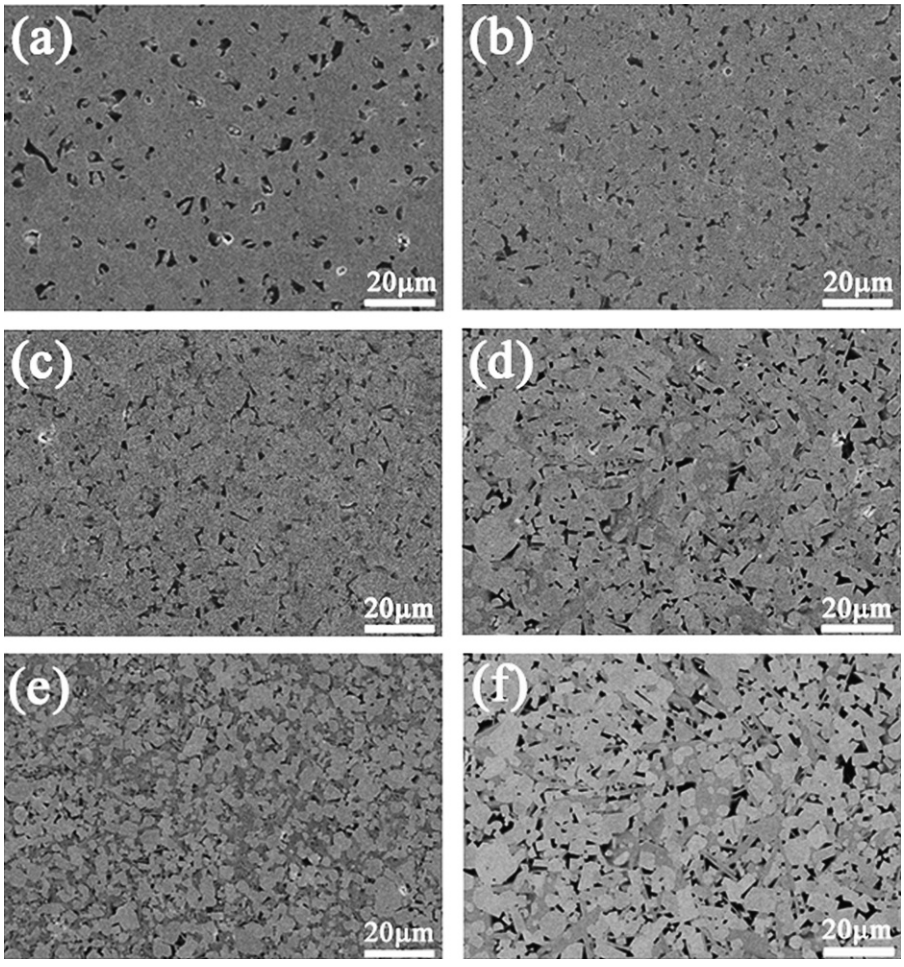

Fig. 3. Scanning electron micrographs showing the polished surfaces of $ZrB_2/Zr_2Al_4C_5$ composites: (a) 0 vol%; (b) 10 vol%; (c) 20 vol%; (d) 30 vol%; (e) 40 vol%; and (f) back scattered electron image of 30 vol% sample.

significantly higher than the starting powder (2.5 μm). Apparently, the presence of ZrO_2 allowed the coarsening of ZrB_2 during heating, which would inhibit its full densification through evaporation–condensation. The average grain size of ZrB_2 in the composite with 10 vol% or more $Zr_2Al_4C_5$ grains was smaller than in the single-phase ZrB_2. This variation in grain size can be also observed in the polished surface of ceramics in Table 1. This indicated that the grains growth of ZrB_2 appeared to be inhibited or pinned by the in situ formed $Zr_2Al_4C_5$, and the restriction of grain growth could further improve the densification and the material's stability at elevated temperature during sintering [34]. On the other hand, the carbon introduced from the starting powders reduced the adverse effect for grain coarsening by removing the oxygen impurities. The removal of oxide impurities was especially efficient during the reaction, promoting the mass transport during the heating process without significant particle coarsening. The results revealed that the in situ $Zr_2Al_4C_5$ layered grains can not only promote the densification of ZrB_2 powder but also inhibit the grain growth of ZrB_2 during the SPS cycle.

Fig. 4 shows the SEM micrographs of fracture surface of $ZrB_2/Zr_2Al_4C_5$ composites with different $Zr_2Al_4C_5$ contents. It can been seen that porosity was hardly observed on the cross-section of composites with $Zr_2Al_4C_5$ particle, and only some small pores trapped into the ZrB_2 grains can be observed. Meanwhile, no trace of layered $Zr_2Al_4C_5$ grain pullout was observed. Besides a decrease in grain size with an increase in $Zr_2Al_4C_5$ amount, a change in fracture modes can be observed. Sample ZA0 exhibited a rather smooth fracture surface, and some pores were detected in Fig. 4(a). Corresponding to a transgranular fracture mode which was also reflected in lower fracture toughness of 2.55 MPa $m^{1/2}$. The fracture surfaces of composites with $Zr_2Al_4C_5$ particle showed a concave–convex appearance (shown in Fig. 4(b)–(e)), and were much rougher than those of the ZA0 sample, which indicated that the fracture modes of the $ZrB_2/Zr_2Al_4C_5$ composites changed from transgranular modes to mixed transgranular and intergranular ones. Therefore, the rough fracture surface of the composites and ragged crack propagation path suggested that the crack deflection should be another toughening mechanism, which was also considered to favor the improvement of the mechanical properties.

Young's modulus measured for the various $ZrB_2/Zr_2Al_4C_5$ composition consolidated by SPS are summarized

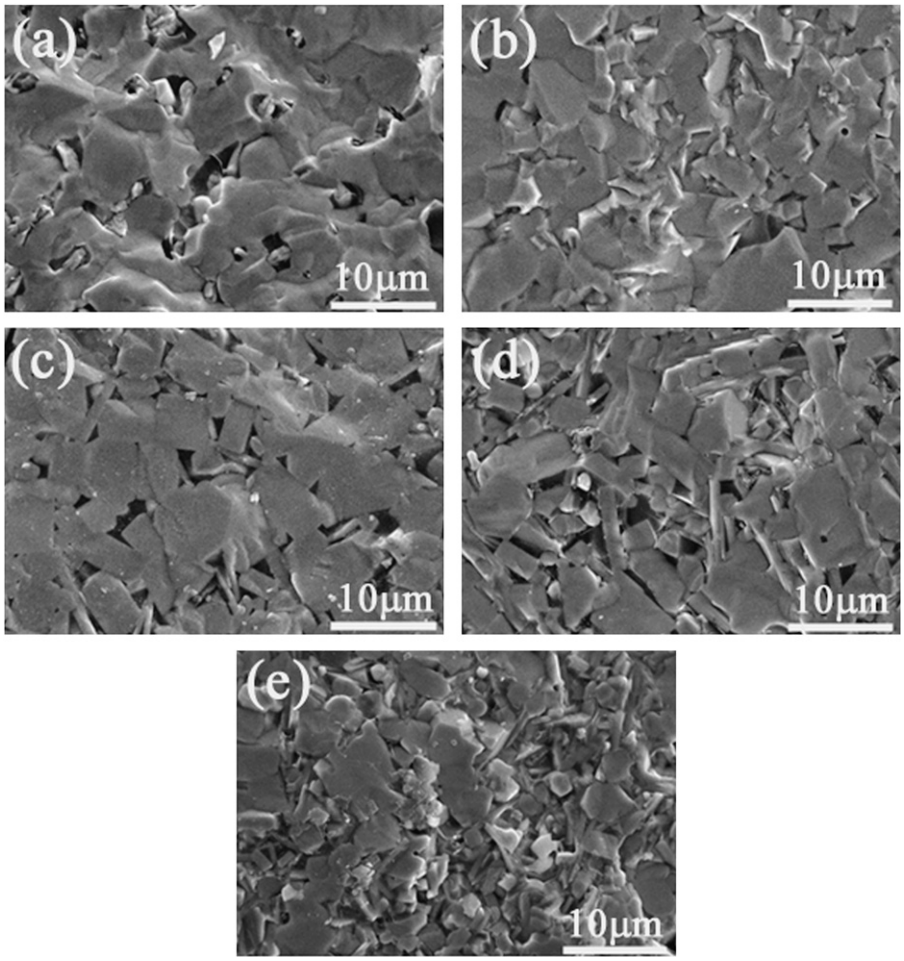

Fig. 4. SEM micrographs of fracture surface of $ZrB_2/Zr_2Al_4C_5$ composites: (a) 0 vol%; (b) 10 vol%; (c) 20 vol%; (d) 30 vol% and (e) 40 vol%.

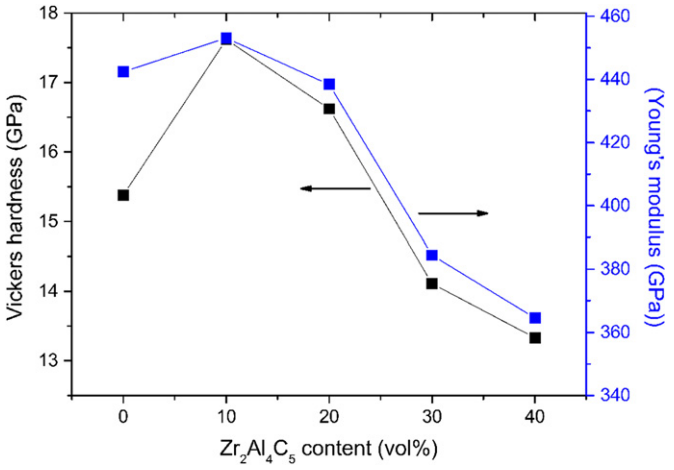

Fig. 5. The curve of the Vickers hardness and Young's modulus in ZrB_2/$Zr_2Al_4C_5$ composites.

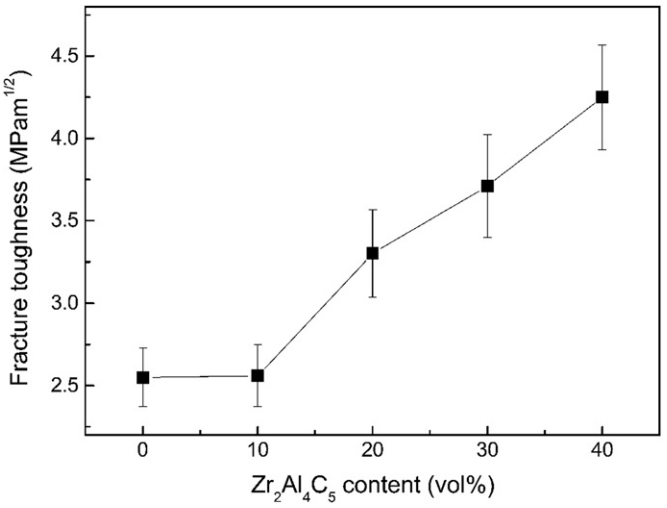

Fig. 6. Fracture toughness of ZrB_2/$Zr_2Al_4C_5$ composites with different $Zr_2Al_4C_5$ contents.

in Fig. 5. From this figure, it can be seen that Young's modulus firstly increased and then decreased with the increasing $Zr_2Al_4C_5$ content. Young's modulus appeared to decrease as the $Zr_2Al_4C_5$ content increased, most probably because of lower intrinsic Young's modulus of $Zr_2Al_4C_5$ compared to ZrB_2. However, Young's modulus of ZA1 higher than that of ZA0 attributing to the lower open porosity (0.12%) of ZA1 sample is shown in Fig. 2. Therefore, the effect of porosity on Young's modulus must also be considered. The relationship between the porosity and Young's modulus is proposed as [35]

$$M = M_0(1-kP) \tag{3}$$

where M_0 is Young's modulus of pore-free materials, k a constant, and P is the volume fraction of porosity in the materials. For example, compared to Young's modulus (363 GPa) of as-received powder compacts, Young's modulus for ZA0 was higher, as the open porosity of ZA0 was lower than that of as-received powder compacts. It was found that Young's modulus of the composites decreased linearly with porosity. This strong relation demonstrates that Young's modulus of the pores-containing composites are mostly dominated by the porosity of the materials. It was indicated that Young's modulus had a close correlation with the additives phases and the porosity in the materials.

From Fig. 5, the Vickers hardness of sintered samples firstly increased and then decreased with the increase in $Zr_2Al_4C_5$ content. Compared to ZrB_2, $Zr_2Al_4C_5$ had a lower Vickers hardness. The literature had reported that the Vickers hardness of a material was in general decreased by the addition of weak second phases, such as carbon/graphite, h-BN [10]. Thus, the Vickers hardness of ZrB_2/$Zr_2Al_4C_5$ composites should be slightly decreased with the increasing $Zr_2Al_4C_5$ content. However, the ZA1 showed a maximum value of hardness of 17.62 GPa. Meanwhile, the lower Vickers hardness of ZA0 is attributed to the ZA0 ceramic that contains some residual porosity (the open porosity was 0.82%). So, the Vickers hardness has been shown to decrease exponentially as the porosity increases for ceramic materials [36].

The fracture toughness values of the compositions are depicted in Fig. 6. It can be seen that the ZrB_2-based composites including $Zr_2Al_4C_5$ grains have markedly higher fracture toughness than the monolithic ZrB_2 material, and the fracture toughness increased with the content of $Zr_2Al_4C_5$ grains. For a monolithic ZrB_2 ceramic fabricated under the same conditions, the fracture toughness was only 2.55 MPa m$^{1/2}$, while the maximum value of fracture toughness reached 4.25 MPa m$^{1/2}$ for ZA4, which was about 70% larger than that of the ZA0 ceramic. To explain the variation in fracture toughness, the microstructures of the all these sintered samples were analyzed in Fig. 3. Comparing the microstructures of ZrB_2/$Zr_2Al_4C_5$ fabricated from the all these different $Zr_2Al_4C_5$ contents, the SEM analysis revealed that the in situ formed $Zr_2Al_4C_5$ grains in the prepared ceramics were predominantly elongated with rods/whiskers-like morphology. For ZA4, the improvement in toughness may have resulted from a relatively fine and homogeneous microstructure and elongated $Zr_2Al_4C_5$ grains, as shown in Fig. 3(e).

The elongation of the $Zr_2Al_4C_5$ particles was evaluated by calculating the aspect ratio of the $Zr_2Al_4C_5$ grains for each material. The dimensions of elongated $Zr_2Al_4C_5$ grains and their aspect ratio are shown in Table 1. The dimensions of elongated $Zr_2Al_4C_5$ grains firstly increased and then gradually decreased with the increase of $Zr_2Al_4C_5$ content. The coarsening of $Zr_2Al_4C_5$ grains in the ZrB_2 matrix after SPS was observed in the ZA2 sample. A quantitative metallographic technique [37], which had been developed to estimate the aspect ratio of elongated silicon nitride grains, was adopted in the present study to determine the aspect ratio of $Zr_2Al_4C_5$ particles. In the sintered composites, the average aspect ratio of the $Zr_2Al_4C_5$ particles increased gradually with the increasing content of the in situ formation of layered $Zr_2Al_4C_5$ grains. The maximum average aspect ratio of $Zr_2Al_4C_5$ grains was

estimated to be 8.5 for ZA4. It was generally believed that elongated grains with large aspect ratio would benefit the fracture toughness [38]. The incorporation of high aspect ratio reinforcements has been indicated to reduce the brittleness of ZrB_2-based composites [39]. These reinforcements, such as carbon fibers, graphite flakes and SiC whiskers, fibers or platelets, reduce brittleness by a combination of toughening mechanisms like debonding, pull-out and bridging as well as enhanced crack deflection and crack pinning. Therefore, the aspect ratio of $Zr_2Al_4C_5$ grains affects the fracture toughness of ceramics. Not only the high aspect ratio of $Zr_2Al_4C_5$ grains but also the weaker interface bonding and weak internal layers existing within the $Zr_2Al_4C_5$ crystal could lead to the crack deflection and bridging [25]. Thus, the addition of $Zr_2Al_4C_5$ layered structure was considered to cause the improvement in toughness.

To elucidate the toughening mechanisms, the propagation path of Vickers indentation induced cracks in the ZrB_2/$Zr_2Al_4C_5$ ceramics is observed by SEM, as shown in Fig. 7. It can be seen that the indentation crack path in the ZA4 grade appeared more tortuous than that of the ZA0 sample. Therefore, the crack path of ZA4 sample became zigzag and prolonged, which indicated that these interactions absorb the energy of crack propagation during the fracture process and lead to a shorter crack path, thus leading to the materials toughening [40]. Inspection of crack propagation revealed that the crack deflection and crack bridging resulted from the layered $Zr_2Al_4C_5$ particles in ZA4, as indicated by the arrows in Fig. 7(a) and (b). These toughening mechanisms increased energy dissipation during crack propagation, and resulted in higher fracture toughness (4.25 MPa $m^{1/2}$). While the crack in material ZA0 (Fig. 7(c)) appeared relatively straight with little or no deflection, which was consistent with declined fracture toughness.

4. Conclusion

$ZrB_2/Zr_2Al_4C_5$ composite ceramics with different volume contents of in situ formed $Zr_2Al_4C_5$ were fabricated by the spark plasma sintering technique at 1800 °C under a pressure of 20 MPa. The densification of ZrB_2 was remarkably improved when 20 vol% $Zr_2Al_4C_5$ was used as a sintering aid. The improvement was mainly attributed to the elimination of oxide layer on the surface of the initial ZrB_2 powders by the addition of carbon from the starting powders and the active Al during sintering process. Higher content of $Zr_2Al_4C_5$ significantly restrained the grain growth of the ZrB_2 matrix, and promoted the average aspect ratio of the $Zr_2Al_4C_5$ grains. With the increase in $Zr_2Al_4C_5$ content, both the Vickers hardness and Young's modulus of composites firstly increased and then decreased. The composite with 40 vol% $Zr_2Al_4C_5$ showed the optimized microstructure and excellent properties, and its fracture toughness value of 4.25 MPa $m^{1/2}$, which was about 70% higher than that of the ZrB_2 ceramic. Higher fracture toughness was mainly attributed to the in situ formed $Zr_2Al_4C_5$ phases and ZrB_2 phase homogeneously dispersing on the whole, and the fracture mode exhibiting a mixture of inter- and intra-granular fractures. The improvement was mainly attributed to toughening mechanisms such as the presence of laminated $Zr_2Al_4C_5$ grains, crack deflection and crack bridging. In addition, the existence of weaker interface bonding and weak internal layers within the $Zr_2Al_4C_5$ inclusions could enhance the fracture toughness of $ZrB_2/Zr_2Al_4C_5$ ceramics.

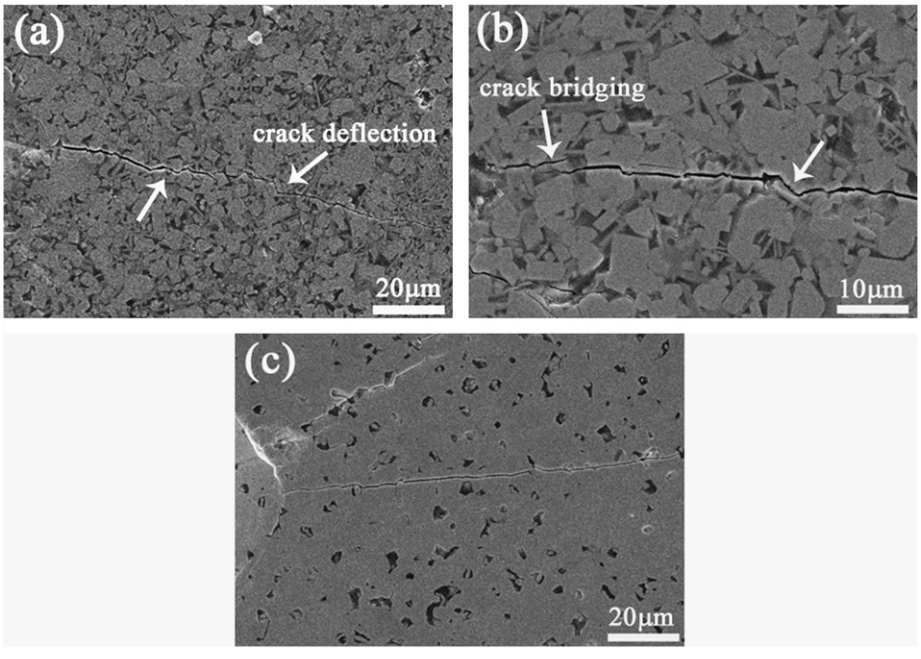

Fig. 7. SEM micrograph of the crack path on the polished surface; (a) and (b) the low and high magnifications of ZA4; (c) ZA0.

References

[1] E. Wuchina, M. Opeka, S. Causey, K. Buesking, J. Spain, A. Cull, J. Routbort, F. Guitierrez-Mora, Designing for ultrahigh-temperature applications: the mechanical and thermal properties of HfB_2, HfCx, HfNx and αHf(N), Journal of Materials Science 39 (2004) 5939–5949.

[2] M.M. Opeka, I.G. Talmy, J.A. Zaykoski, Oxidation-based materials selection for 2000 °C + hypersonic aerosurfaces: theoretical considerations and historical experience, Journal of Materials Science 39 (2004) 5887–5904.

[3] A.L. Chamberlain, W.G. Fahrenholtz, G.E. Hilmas, D.T. Ellerby, High-strength zirconium diboride-based ceramics, Journal of the American Ceramic Society 87 (2004) 1170–1172.

[4] W.G. Fahrenholtz, G.E. Hilmas, Refractory diborides of zirconium and hafnium, Journal of the American Ceramic Society 90 (2007) 1347–1364.

[5] F. Monteverde, The thermal stability in air of hot-pressed diboride matrix composites for uses at ultra-high temperatures, Corrosion Science 47 (2005) 2020–2033.

[6] F. Monteverde, A. Bellosi, Microstructure and properties of an HfB_2–SiC composite for ultra high temperature Applications, Advanced Engineering Materials 6 (2004) 331–336.

[7] H. Pastor, Metallic borides: preparation of solid bodies. Sintering methods and properties of solid bodies, in: V.I. Matkovich (Ed.), Boron and Refractory Borides, Springer, New York, 1977, pp. 457–493.

[8] S.Q. Guo, Densification of ZrB_2-based composites and their mechanical and physical properties: a review, Journal of the European Ceramic Society 29 (2009) 995–1011.

[9] Y. Wang, J. Liang, W. Han, X. Zhang, Mechanical properties and thermal shock behavior of hot-pressed ZrB_2–SiC–AlN composites, Journal of Alloys and Compounds 475 (2009) 762–765.

[10] H.T. Wu, W.G. Zhang, Fabrication and properties of ZrB_2–SiC–BN machinable ceramics, Journal of the European Ceramic Society 30 (2010) 1035–1042.

[11] A. Balbo, D. Sciti, Spark plasma sintering and hot pressing of ZrB_2–$MoSi_2$ ultra-high-temperature ceramics, Materials Science and Engineering A 475 (2008) 108–112.

[12] S.Q. Guo, Y. Kagawa, T. Nishimura, H. Tanaka, Pressureless sintering and physical properties of ZrB_2-based composites with $ZrSi_2$ additive, Scripta Materialia 58 (2008) 579–582.

[13] W.W. Wu, G.J. Zhang, Y.M. Kan, P.L. Wang, Reactive hot pressing of ZrB_2–SiC–ZrC composites at 1600 °C, Journal of the American Ceramic Society 91 (2008) 2501–2508.

[14] Y.G. Wang, M. Zhu, L.F. Cheng, L.T. Zhang, Fabrication of SiCw reinforced ZrB_2-based ceramics, Ceramics International 36 (2010) 1787–1790.

[15] S. Guicciardi, L. Silvestroni, M. Nygren, D. Scitiw, Toughened ZrB_2-based ceramics through SiC whisker or SiC chopped fiber additions, Journal of the American Ceramic Society 93 (2010) 2384–2391.

[16] J. Lin, X.H. Zhang, Z. Wang, W.B. Han, Microstructure and mechanical properties of ZrB_2–SiC–ZrO_{2f} ceramic, Scripta Materialia 64 (2011) 872–875.

[17] Q. Liu, W.B. Han, P. Hu, Microstructure and mechanical properties of ZrB_2–SiC nanocomposite ceramic, Scripta Materialia 61 (2009) 690–692.

[18] F.Y. Yang, X.H. Zhang, J.C. Han, S.Y. Du, Mechanical properties of short carbon fiber reinforced ZrB_2–SiC ceramic matrix composites, Materials Letters 62 (2008) 2925–2927.

[19] W.B. Tian, Y.M. Kan, G.J. Zhang, P.L. Wang, Effect of carbon nanotubes on the properties of ZrB_2–SiC ceramics, Materials Science and Engineering A 487 (2008) 568–573.

[20] X. Zhang, P. Zhou, P. Hu, W. Han, Toughening of laminated ZrB_2–SiC ceramics with residual surface compression, Journal of the European Ceramic Society 31 (2011) 2415–2423.

[21] P. Zhou, P. Hu, X.H. Zhang, W.B. Han, Laminated ZrB_2–SiC ceramic with improved strength and toughness, Scripta Materialia 64 (2011) 276–279.

[22] J.W. Zimmermann, G.E. Hilmas, W.G. Fahrenholtz, Thermal shock resistance and fracture behavior of ZrB_2-based fibrous monolith ceramics, Journal of the American Ceramic Society 92 (2009) 161–166.

[23] L.Y. Zheng, F.Z. Li, Y.C. Zhou, Preparation, microstructure, and mechanical properties of TiB_2 using Ti_3AlC_2 as a sintering aid, Journal of the American Ceramic Society 95 (2012) 2028–2034.

[24] Y.L. Chin, W.H. Tuan, J.L. Huang, C.A. Wang, Toughening alumina with layered Ti_3SiC_2 inclusions, Journal of Alloys and Compounds 491 (2010) 477–482.

[25] R.B. Zhang, G.Q. Chen, W.B. Han, Synthesis, mechanical and physical properties of bulk $Zr_2Al_4C_5$ ceramic, Materials Chemistry and Physics 119 (2010) 261–265.

[26] K. Sugiura, T. Iwata, H. Yoshida, S. Hashimoto, K. Fukuda, Syntheses, crystal structures and Si solubilities of new layered carbides $Zr_2Al_4C_5$ and $Zr_3Al_4C_6$, Journal of Solid State Chemistry 181 (2008) 2864–2868.

[27] Q.L. Guo, J.G. Li, Q. Shen, L.M. Zhang, Toughening of ZrB_2–SiC ceramics with the micro-structure ZrB_2/Zr–Al–C fibrous monolith, Scripta Materialia 66 (2012) 296–299.

[28] G.D. Quinn, J. Salem, I. Bar-on, Fracture toughness of advanced ceramics at room temperature, Journal of Research of the National Institute of Standards and Technology 97 (1992) 579–607.

[29] R.B. Zhang, G.Q. Chen, Y.M. Pei, D.N. Fang, Thermal stability of bulk $Zr_2Al_4C_5$ ceramic at elevated temperatures, International Journal of Refractory Metals and Hard Materials 30 (2012) 102–106.

[30] A.L. Chamberlain, W.G. Fahrenholtz, G.E. Hilmas, Pressureless sintering of zirconium diboride, Journal of the American Ceramic Society 89 (2006) 450–456.

[31] S.M. Zhu, W.G. Fahrenholtz, G.E. Hilmas, S.C. Zhang, Pressureless sintering of carbon-coated zirconium diboride powders, Materials Science and Engineering A 459 (2007) 167–171.

[32] F. Monteverde, S. Guicciardi, A. Bellosi, Advances in microstructure and mechanical properties of zirconium diboride based ceramics, Materials Science and Engineering A 346 (2003) 310–319.

[33] M. Ikegami, S.Q. Guo, Y. Kagawa, Densification behavior and microstructure of spark plasma sintered ZrB_2-based composites with SiC particles, Ceramics International 38 (2012) 769–774.

[34] S.K. Tadokoro, E.N.S. Muccillo, Physical characteristics and sintering behavior of ultrafine zirconia-ceria powders, Journal of the European Ceramic Society 22 (2002) 1723–1728.

[35] E.A. Dean, J.A. Lopez, Empirical dependence of elastic moduli on porosity for ceramic materials, Journal of the American Ceramic Society 66 (1983) 366–370.

[36] V. Milman, S.I. Chugnova, I.V. Goncharova, T. Chudoba, W. Lojkowski, W. Gooch, International Journal of Refractory Metals and Hard Materials 17 (1999) 361–368.

[37] G. Wotting, B. Kanka, G. Ziegler, in: S. Hampshire (Ed.), Non-oxide Technical and Engineering Ceramics, Elsevier Applied Sci., London, 1986, pp. 83–90.

[38] X.H. Zhang, L. Xu, S.Y. Du, C.Y. Liu, J.C. Han, W.B. Han, Spark plasma sintering and hot pressing of ZrB_2–SiC_W ultra-high temperature ceramics, Journal of Alloys and Compounds 466 (2008) 241–245.

[39] L. Silvestroni, D. Sciti, C. Melandri, S. Guicciardi, Toughened ZrB_2-based ceramics through SiC whisker or SiC chopped fiber additions, Journal of the European Ceramic Society 30 (2010) 2155–2164.

[40] J. Rodel, Interaction between crack deflection and crack bridging, Journal of the European Ceramic Society 10 (1992) 143–150.